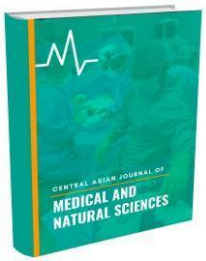

CENTRAL ASIAN JOURNAL OF MEDICAL AND NATURAL SCIENCES
https://cajmns.casjournal.org/index.php/CAJMNS
Volume: 07 Issue: 04 | October 2026 ISSN: 2660-4159

Article

Effect of bulk Defect Concentration on Capacitance Characteristics of an Experimentally Calibrated CIGS Solar Cell Using SCAPS-1D via Admittance Spectroscopy

Ahmed K. Marei*[1], Ayed N. Saleh[2]

1,2. Department of Physics, College of Education for Pure Science, University of Tikrit, Iraq
*Correspondence: akmueps76@st.tu.edu.iq

Abstract: In this work, the combined effect of temperature (184–304 K) and defect concentration (1.4×10^{12}–1.4×10^{16} cm^{-3}) on the capacitance characteristics of a calibrated Cu(In,Ga)Se_2 (CIGS) solar cell was systematically investigated using Solar Cell Capacitance Simulator in one dimension (SCAPS-1D) via admittance spectroscopy. The results show that the characteristic frequency shifts significantly with temperature from approximately (~3.7×102 Hz) at (184 K) to (~5.1× 106 Hz) at (304 K), indicating a thermally activated emission process spanning nearly three orders of magnitude. Meanwhile, increasing defect concentration reduces the low-frequency capacitance from (~65.7 nF/cm²) to (~61.4 nF/cm²) and enhances the visibility of the defect response without altering its intrinsic energy level. The derivative analysis ($-f \times dC/df$) enabled precise extraction of the characteristic frequencies, especially at high defect concentration (1.4×10^{16} cm^{-3}), where sharp and well-defined peaks were observed. The Arrhenius analysis yielded an activation energy of (0.328 eV), which is lower than the introduced defect level (0.88 eV), reflecting the effective emission barrier relative to the conduction band. These findings confirm that temperature controls the dynamic defect response, while defect concentration primarily governs the amplitude and detectability, providing a reliable framework for defect characterization and optimization of CIGS solar cells.

Keywords: CIGS Solar Cells, SCAPS-1D, Admittance Spectroscopy, Bulk Defects, Activation Energy

Citation: Marei, A. K., Saleh, A. N. Effect of bulk Defect Concentration on Capacitance Characteristics of an Experimentally Calibrated CIGS Solar Cell Using SCAPS-1D via Admittance Spectroscopy. Central Asian Journal of Medical and Natural Science 2026, 7(4), 54-65.

Received: 20th Apr 2026
Revised: 11th May 2026
Accepted: 19th June 2026
Published: 15th July 2026

1. Introduction

Solar energy is one of the most sustainable and efficient means of satisfying the world power demand, and the progress in photovoltaic (PV) technologies is growing so rapidly that greater and broader application is possible. In the field of thin-film (PV), the (CIGS) cells offer a remarkable performance; a significant energy conversion ratio of 23.35% achieved recently has been reported in addition to remarkable light absorption and long-term stability [1, 2]. These benefits render CIGS to be a promising candidate to deploy for the renewables on both a domestic scale and the worldwide scale. Nevertheless, the performance of CIGS cells is still severely limited because of defects in the absorption layer and at heterogeneously integrated junction interfaces [3]. In particular, deep defects act as efficient recombination centers and charge retention sites, shortening the lifetime of charge carriers and deteriorating the vital (PV) parameters such as open circuit voltage, fill factor among others [4]. Hence, a deep understanding of defect states and their influence on the electrical response is crucial if one expects to get more performance enhancement

of the device. These capacitance characterization approaches, which are particularly prominent in admittance spectroscopy, are regarded as viable approaches towards the characterization of electrically driven defect states in semiconductors [5]. By assessing the frequency- and temperature-dependent capacitance response, fundamental defect parameters, such as activation energy, and also some key performance metrics, can be deduced. Experimental measurements are frequently influenced by parasitic phenomena such as series resistance and a combination of interface states that may disguise an intrinsic defect response and present difficulties for measuring its actual physical behavior. For these reasons numerical simulation has been introduced as a basic methodology to study defect-induced components in photovoltaic equipment [6]. Especially for thin film solar cells, the (SCAPS-1D) simulator models charge transport, recombination process, and defect effects at the level of the device in a controlled environment. After adequate calibration in relation to measured data, SCAPS-1D offers a robust basis to study the innate impact of volumetric defects as well as to study their effect on electrical characteristics. When calibrated with experimental data, SCAPS-1D is a method that is particularly well suited to isolating intrinsic effects of volumetric defects with studies on electrical properties [5, 7]. The current research aims to develop and calibrate a one-dimensional numerical model using the experimentally proven (SCAPS-1D) software for CIGS-made solar cells to estimate the effect of defect Concentration in the material on its capacitive properties through admittance spectroscopy to obtain the capacitance-frequency (C-f) curve and the frequency-capacitance derivative spectrum at different temperatures to determine the characteristic frequency and then extract the activation energy of the dominant defect level through Arrhenius analysis.

2. Numerical simulation

Numerical simulations are used to study the effect of electrical parameters on solar cell performance without the need for experiments. They are also used to characterize solar photovoltaic devices. In this work, we take advantage of the SCAPS-1D version 3.3.12 to perform the numerical simulations. The SCAPS-1D uses the finite difference method with well-defined boundary conditions to solve the fundamental equations: Poisson's equation (1), electron continuity equation (2), hole continuity equation (3), and drift-diffusion equations (4) and (5) presented below. This software was chosen because of the good agreement between the results of numerical simulations performed using the SCAPS-1D and the experimental results [5].

Poisson's equation describes distribution of electrical voltage inside a solar cell [8]:

$$\nabla^2\phi = -\frac{q}{\varepsilon}(p - n + N_D^+ - N_A^- + N_t) \quad (1)$$

Where ϕ, q, ε, p, n, N_D^+, N_A^-, and N_t are the electrostatic potential, elementary charge, material permittivity, and hole, electron, donor, acceptor, and defect Concentrations, respectively.

The continuity equations describe the conservation of charge carriers within the layers [8]:

$$\frac{dn}{dt} = (\frac{1}{q})\nabla.J_n + G_n - R_n \quad (2)$$

$$\frac{dp}{dt} = -(\frac{1}{q})\nabla.J_p + G_p - R_p \quad (3)$$

Where J_n, J_p, G_n, G_p, R_n, and R_p are the electron current concentration, hole current concentration, electron generation rate, hole generation rate, electron recombination rate, and hole recombination rate, respectively.

The carrier transport is described using the drift–diffusion approach, where the total current results from two physical contributions: motion driven by the electric field (drift) and motion caused by Concentration gradients (diffusion) [8]:

$$J_n = q(\mu_n nE + D_n \nabla_n) \quad (4)$$

$$J_p = q(\mu_p PE + D_p \nabla_p) \quad (5)$$

Where μ_n, μ_p, D_n, and D_p are the electron mobility, hole mobility, electron diffusion coefficient, and hole diffusion coefficient, respectively. This model is widely used in thin-film solar cell simulations, because it captures effectively the carrier transport behavior for typical device operating fields and mobility ranges.

The Shockley–Read–Hall (SRH) recombination equation describes the electron–hole recombination rate [9]:

$$R_{SRH} = \frac{np - n_i^2}{\left[\tau_p(n + n_1) + \tau_n(p + p_1)\right]} \quad (6)$$

Where R_{SRH}, n_i, τ_n, τ_p, n_1, and p_1 are the recombination rate, intrinsic carrier Concentration, electron lifetime, hole lifetime, and the effective electron and hole Concentrations associated with the defect energy level, respectively.

The power conversion efficiency η is defined as [10]:

$$\eta = \frac{V_{oc}.J_{sc}.FF}{P_{in}} \quad (7)$$

Where η, V_{oc}, J_{sc}, FF, and P_{in} are the power conversion efficiency, open-circuit voltage, short-circuit current concentration, fill factor, and incident light power density, respectively.

The fill factor is used to evaluate the solar cell performance [11]:

$$FF = \frac{V_{mpp}.J_{mpp}}{V_{oc}.J_{sc}} \quad (8)$$

Where V_{mpp} and J_{mpp} are the voltage at the maximum power point and the current density at the maximum power point.

The current of the solar cell can be estimated using formula [11]:

$$I = I_o(\exp(\frac{qV}{KT}) - 1) \quad (9)$$

Where I, I_o, V, K, and T are the output current of the solar cell, reverse saturation current, applied voltage, Boltzmann's constant, and absolute temperature, respectively.

The open-circuit voltage V_{oc} can be estimated using the following equation [11]:

$$V_{oc} = \frac{KT}{q}\ln(\frac{I_{sc}}{I_o} + 1) \quad (10)$$

2.1. Device structure and material parameters

This paper develops a numerical device design based on a high-efficiency CIGS solar cell, as proposed by Garris et al. [12]. This model builds a realistic structure with a base of glass/molybdenum/CIGS/CdS/i-ZnO/ZnO:Al. Experimental results show that deep defects in the absorption layer, particularly hole traps with defect energies ranging from (0.5 to 0.9 eV), have a great influence on capacitive response and charge carrier dynamics. Hence, the numerical model was adjusted in the present study in order to be physically consistent with the experimental data. The previous step was calibration by matching simulated charge carrier concentration, current-voltage density and quantum efficiency profiles with experimental data to build a valid model. Using this experimentally calibrated design, this simulation provides a physically meaningful framework for studying the defect-controlled electrical behavior. In particular, we investigate the effect of defect Concentration in the material on the device's dynamic response using capacitive-frequency (C-*f*) analysis under varying temperatures. Therefore, through it, the characteristic frequency of the defects can be found and then the defect activation energy (E_A) can be extracted.

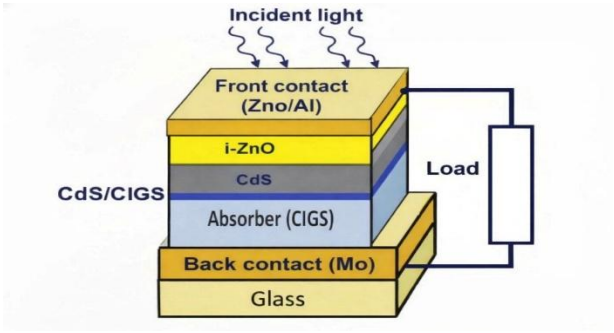

Figure 1. Schematic representation of the calibrated CIGS thin-film solar cell structure employed in SCAPS-1D simulations.

The material parameters and defect properties used in the simulation are summarized in Table 1. By employing an experimentally validated device architecture as the baseline structure, the simulation provides a physically meaningful framework for investigating defect-controlled electrical behavior [12-14].

Table 1. Parameters used to simulate the CIGS solar cell.

Layers properties	i-ZnO	n-Cds	p-CIGS
Thickness (nm)	50	50	2300
Dielectric relative Permittivity	9	10	13.6
Electron affinity (eV)	4.5	4.2	4.5
Band gap (eV)	3.3	2.4	1.2
Effective density of state in C_B	$2.200x10^{18}$	$2.200x10^{18}$	$2.200x10^{18}$
Effective density of state in V_B	$2.200x10^{18}$	$2.200x10^{18}$	$2.200x10^{18}$
Electron thermal velocity (cm/s)	$1x10^{7}$	$1x10^{7}$	$1x10^{7}$
Hole thermal velocity (cm/s)	$1x10^{7}$	$1x10^{7}$	$1x10^{7}$
Electron mobility($cm^2.V^{-1}.s^{-1}$)	100	100	100
Hole mobility ($cm^2.V^{-1}.s^{-1}$)	25	25	25
Donor concentration (cm^{-3})	$1x10^{15}$	$1x10^{17}$	$1x10^{10}$
Acceptor concentration (cm^{-3})	$1x10^{10}$	$1x10^{10}$	$1.5x10^{16}$
Bulk defect properties (CIGS absorber)			
Bulk defect Concentration (cm-	0	0	$1.4x10^{12}$-
Capture cross-section electrons	0	0	$2.5x10^{-14}$
Capture cross-section holes	0	0	$2.5x10^{-14}$

Defect energy level (eV)	-	-	Ev+0.88
Defect type	-	-	Acceptor-like
Defect charge state	-	-	-1/-2
Energy distribution	-	-	Gaussian
characteristic energy (eV)	-	-	0.1
Interface defect properties (CIGS/CdS junction)			
Interface defect concentration		$1x10^{13}$	
Capture cross-section electrons		$3x10^{-14}$	
Capture cross-section holes		$3x10^{-14}$	
Defect energy level (eV)		Ec-0.27	
Defect type		Donor-like	

2.2. Simulation Conditions and Model calibration

The device design and material parameters were based on a high-efficiency CIGS solar cell, which has been successfully studied and published in the scientific literature by Garris et al. [12]. This enabled the design of a realistic device that accurately mimics real CIGS thin-film technology. The model was first calibrated by introducing a dominant defect level of (1.4×10^{15} cm^{-3}) in the CIGS absorber layer, along with a (0.88 eV) energy location in the band gap and a (2.5×10^{-14} cm^2) capture cross-section Garris et al. [12]. This allowed for the re-simulation of experimentally observed recombination and the practical performance of the photovoltaic cells. Furthermore, a surface defect was introduced at the (CIGS/CdS) junction to ensure the ability to characterize the surface recombination mechanisms common in high-efficiency CIGS devices, the characteristics of which are shown in Table 1, and to allow for the accurate reproduction of the current-voltage characteristics in the simulation and experiment to calibrate the results. Note that the current density and voltage characteristics were simulated under standard AM1.5G illumination at (294 K), including a series resistance of ($0.3\ \Omega \cdot cm^2$) and a sub-resistance of ($10^4\ \Omega \cdot cm^2$) to represent resistive loss. After obtaining satisfactory measurements and confirming the model's calibration, the surface defect was deliberately excluded from the model to monitor the underlying contribution of the underlying defects in the absorption layer. This approach allowed all other solar cell outputs, capacitance response, and impedance spectra to be related solely to the mechanical properties of the material defect, thus eliminating the effects of surface recombination and improving the physical interpretation. Subsequently, all capacitance analyses and impedance spectroscopy measurements were performed in the dark to isolate the charge exchange processes resulting from the defects from the photo charge carriers. Temperature-dependent impedance spectroscopy measurements were performed within a frequency range of (1 Hz) to (10^7 Hz) and a temperature range of (184 K) to (304 K) in (30 K) steps under a constant forward bias voltage of (0.7 V) and varying defect Concentrations from (1.4×10^{12} cm^{-3}) to (1.4×10^{16} cm^{-3}). Frequency shifts were analyzed using Arrhenius relations and defect activation energy.

2.3. Admittance spectroscopy under temperature variations for defect activation energy determination

Admittance $\Upsilon(\omega)$ of the device can be modeled as a parallel combination of a conductance and a capacitance, both of which vary with the applied measurement frequency. Accordingly, the admittance can be written as [15]:

1. $$\Upsilon(\omega) = G(\omega) + j\,\omega C(\omega) \qquad (11)$$

Where $G(\omega)$,and $C(\omega)$ represents the frequency-dependent conductance, and corresponding capacitance component.

These two quantities are not independent; rather, they are mathematically related through the Kramers–Kronig relations. Such relations demonstrate that the information obtained from the conductance spectrum is equivalent to that derived from the capacitance spectrum, allowing either quantity to be used for defect analysis [16].

In the CIGS heterojunction solar cells, the total measured capacitance cannot be described solely by the ideal depletion capacitance of an abrupt p–n junction. Instead, it consists of several physical contributions arising from the depletion region, excess carrier storage, bulk defect states, and interface traps. Accordingly, the total capacitance is expressed as [7]:

$$C_{total} = \sqrt{\frac{\varepsilon_{eff} qN}{(V_{bi} - V)^2}} + \frac{1}{\sqrt{j\omega\tau + 1}} \frac{q^2 L \Delta n}{KT} + \ln(1+\omega^2\tau_t^2) \frac{q^2 N}{2\omega^2 \tau_t KT} + \tan^{-1}(\omega\tau_i) \frac{iq^2 D}{KT} \quad (12)$$

Where C_{total}, ε_{eff}, N, V_{bi}, ω, τ, τ_t, τ_i, L, and D represent the total capacitance of the device, the effective dielectric permittivity of the absorber layer, the elementary charge, the doping concentration, the built-in potential, the angular frequency, the characteristic carrier response time, the bulk trap emission time constant, the interface trap time constant, the carrier diffusion length, and the carrier diffusion coefficient, respectively.

The first term is the depletion capacitance in the space-charge region. The second term considers carrier diffusion effects. The third term is for bulk trap contributions and the last term describes interface-related charge exchange processes. In the CIGS devices, increasing bulk defect Concentration will increase the trap-related contribution, and thereby change the apparent doping concentration extracted from C–V profiling.

However, the capacitance measured is usually affected by parasitic series resistance R_s which introduces frequency-dependent attenuation and can lead to an underestimation of the intrinsic capacitance. The corrected capacitance is calculated using the formula to remove this distortion [7]:

$$C = \frac{C_m}{1 + (\omega R_s C_m)^2} \quad (13)$$

Where C and C_m are the corrected capacitance and the measured capacitance, respectively. This correction ensures that the extracted capacitance reflects the intrinsic depletion and defect-related contributions rather than resistive measurement artifacts. In the present calibrated SCAPS-1D study, the combined use of Eqs. (11) and (12) enables accurate evaluation of the impact of bulk defect Concentration on the electrical and capacitance characteristics of the CIGS solar cells.

When an alternating voltage is applied to the device, certain defect levels will periodically catch charge carriers and then let them go as the Fermi level oscillates around the trap energy level. This dynamic response takes place only when the excitation frequency is comparable to or lower than carrier capture and emission rates. If the frequency it applies goes beyond these rates, then defect states will not follow the external signal and so they will no longer contribute to the measured capacitance C_{total}. The characteristic response frequency of a defect is given by the emission time constant of those trapped carriers and can be expressed as [17]:

2. $$f_o = \frac{1}{2\pi} \sigma \nu_{th} N_\nu \exp^{(\frac{-E_A}{KT})} \quad (14)$$

Where f_o, σ, ν_{th}, N_ν, and E_A represent the characteristic frequency of the defect, the capture cross-section of the defect, the thermal velocity of holes, the effective density of states in the valence band, and the activation energy of the defect level, respectively.

Since the thermal velocity and the effective density of states are temperature dependent, their product is approximately proportional to T^2. Therefore, the emission rate can be rewritten in the following form [17]:

$$f_o = 2\xi_o T^2 \exp(\frac{-E_A}{KT}) \quad (15)$$

Where $f_\circ$ represents frequency associated with the defect response and ξ_o is the pre-exponential factor related to the capture cross section and other material parameters.

Taking the natural logarithm of both sides gives:

$$\ln(\frac{f_o}{T^2}) = -\frac{E_A}{K}\frac{1}{T} + \ln(2\xi_o) \quad (16)$$

This equation represents the basis for constructing the Arrhenius plot. By plotting $\ln(\frac{f_o}{T^2})$ as a function of $\frac{1}{T}$, a straight line is obtained. The slope of this line corresponds to $-\frac{E_A}{K}$, from which the activation energy of the defect level can be determined. The intercept provides information about the pre-exponential factor ξ_o, which is related to the capture cross-section of the defect.

Using this method, the activation energies of different defect levels present in the absorber layer or at the heterojunction interface can be extracted from admittance spectroscopy measurements.

3. Results and Discussion

3.1. Calibration of the numerical model by experimental–simulation matching

Figure 2 demonstrates the comprehensive calibration of the numerical model by checking the experimental measurements of the cell investigated by Garris et al. [12] with simulation results for the high-efficiency CIGS solar cell. The J–V curve of the data is able to match with theoretical values obtained for the entire voltage range and closely agrees well with the experimental data in both short- and open-circuit regions (see Fig. 2a). The differences we observed near the short-circuit current can be due to unavoidable experimental conditions as the series resistance effects, recombination at the interface, and imperfect contact behavior, which are difficult to simulate numerically. Moreover, the matching results for the quantum efficiency simulated in Fig. 2b. The response spectrum matches well over the entire wavelength frame, proving that the model truly reflects the light absorption, charge carrier generation, and collection processes. Optical losses at short wavelengths account for a small fall in the experimental quantum efficiency; such loss is due to optical losses at the window and at the dielectric layers, and differences at longer wavelengths are due to losses associated with recombination in bulk mass in the absorber material as well as losses at the back conductor. Additionally, Fig. 2c, which illustrates the charge carrier density distribution obtained from the simulated capacitance response, largely coincides with the experimentally measured charge carrier distribution as a function of the depletion region width. It supports the robustness of the doping concentration and junction depth assumed in the simulation. The small differences at low depletion region widths result primarily from the impact of interface states and deep-plane defects on experimental capacitance tests, although they are only estimated from the numerical model. In general, the excellent agreement of the experimental and simulation results for the electrical, optical, and capacitance-related properties confirm the confidence that the material parameters, interface characteristics, and defect distributions can be

verified, which means the development and analysis of devices can be assured once again. The extracted photovoltaic properties such as the open circuit voltage V_{oc}, short circuit current density J_{sc}, fill factor FF, and efficiency η are presented in Table 2. The simulated results are very similar with the experimental results, and only slight differences are found for J_{sc} and FF.

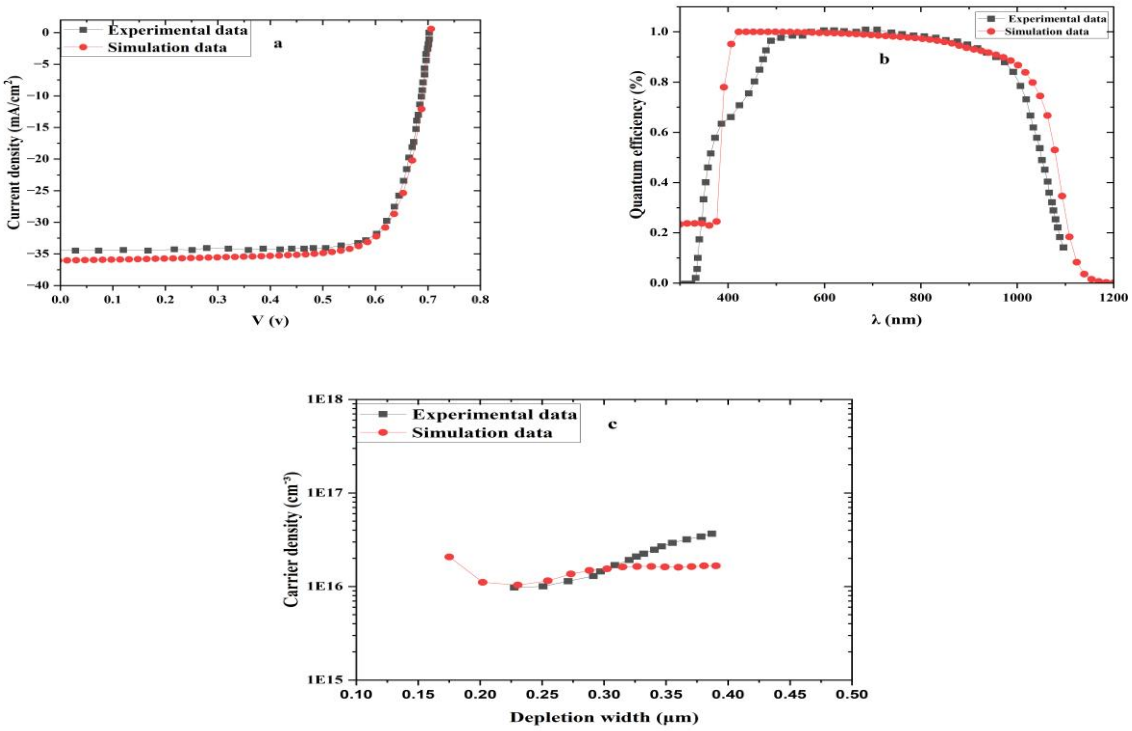

Figue 2. Comparison of the simulated current density–voltage (J–V) characteristics (a), quantum efficiency (QE) spectra (b), and carrier concentration profiles (c) of the CIGS solar cell with the experimental results obtained by Garris et al. [12].

Table 2. Comparison of the Simulated Photovoltaic Performance Parameters of the CIGS Solar Cell with the Experimental Results Obtained by Garris et al. [12].

Model	V_{OC} (V)	J_{SC} (mA/cm²)	FF (%)	η (%)
Experimental	0.701	34.3	80.7	19.4
Simulation data	0.701	36.86	75.05	19.42

3.2. Admittance Spectroscopy and Activation Energy

Figures 3(a-e) show the relationship between amplitude and frequency in the system as both temperature (184–304 K) and defect Concentration (1.4×10^{12}–1.4×10^{16} cm^{-3}) are varied. A distinct three-zone behavior is observed as the defect Concentration changes. At low frequencies ($f \approx 1$–10^2 Hz), the capacitance is nearly constant, decreasing from about (65.7 nF/cm²) at (1.4×10^{12} cm^{-3}) to about (61.4 nF/cm²) at (1.4×10^{16} cm^{-3}) (at 304 K), implying a (6–7%) decrease attributable to increased trap-assisted recombination. At intermediate frequencies ($f \approx 10^3$–10^5 Hz), the capacitance decreases markedly from about (49.8 nF/cm²) to about (41–45 nF/cm²) with increasing defect Concentration. This varies considerably with temperature: from about (10^3–10^4 Hz) at (184 K) to (10^5–10^6 Hz) at (304 K), representing a change of two to three orders of magnitude in absolute values. These patterns are thought to be related to thermally activated charge carrier emission from defect states, according to Shockley-Red-Hall (SRH) statistics, where the emission rate increases with temperature. At high frequencies ($f \geq 10^6$–10^7 Hz), the capacitance converges to approximately (39.6–42.3 nF/cm²) for all temperatures and defect Concentrations,

indicating that the defect states are unable to follow the AC signal, and thus the depletion capacitance dominates the response. Importantly, temperature determines the position of the transition frequency; however, the defect Concentration has a fundamental effect on the magnitude of the capacitance, thus confirming the clear separation between the effects of intrinsic defect energy and the effects of defect concentration [17].

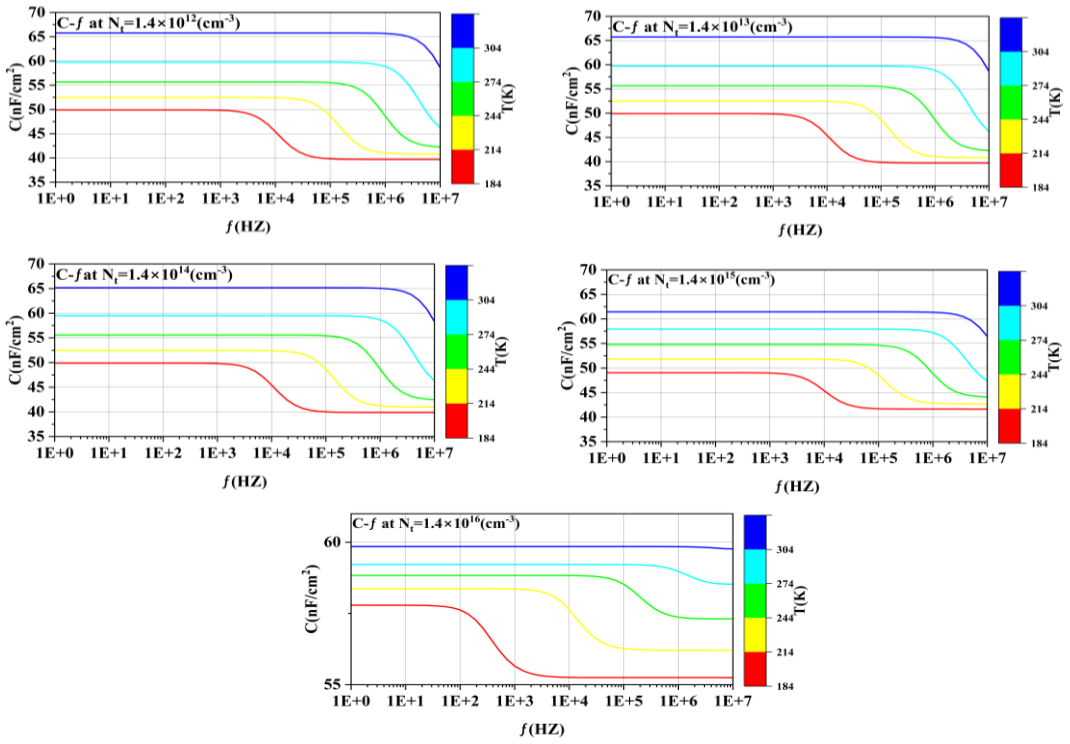

Figure 3. Temperature-Dependent capacitance (C–*f*) characteristics of the CIGS solar cell under Temperatures at a different bulk defect Concentration (a)- $N_t = 1.4 \times 10^{12}$ cm^{-3}, (b)- $N_t = 1.4 \times 10^{13}$ cm^{-3} (c)- $N_t = 1.4 \times 10^{14}$ cm^{-3} (d)- $N_t = 1.4 \times 10^{15}$ cm^{-3} (e)- $N_t = 1.4 \times 10^{16}$ cm^{-3}.

Unlike the raw (C–*f*) curves, measurements of the derivative result in the existence of discrete peaks, corresponding to the relaxation frequency typical of the dominant defect level. These peaks also are systematic in nature, varying from (~3.7×10^2 Hz) at (184 K) to (~1.3×10^4 Hz) at (214 K), (~1.9×10^5 Hz) at (244 K), (~1.3×10^6 Hz) at (274 K), and (~5.1×10^6 Hz) at (304 K), representing quite nearly three orders of magnitude range. This concordance with SRH recombination theory indicates that the emission time constant is reduced exponentially with temperature. Thus it can be seen that the peak amplitude and sharpness correspond to the contribution of defect Concentration. Also at low defect Concentrations (≤10^{15} cm^{-3}) the peaks are weak and wide, which makes its characteristic frequency hard to find. The sharper and well-defined peaks at higher levels, in particular those at (1.4×10^{16} cm^{-3}), vastly improve the accuracy of frequency measurement. The improvement in the defect response, as the defect concentration increases, is indicative of this fact in that the defect response itself has no major increase in energy level. Therefore, the derivative approach is necessary to distinguish defect signal from capacitance contributions caused by the background and was essential to calculation of activation energy of our application [17].

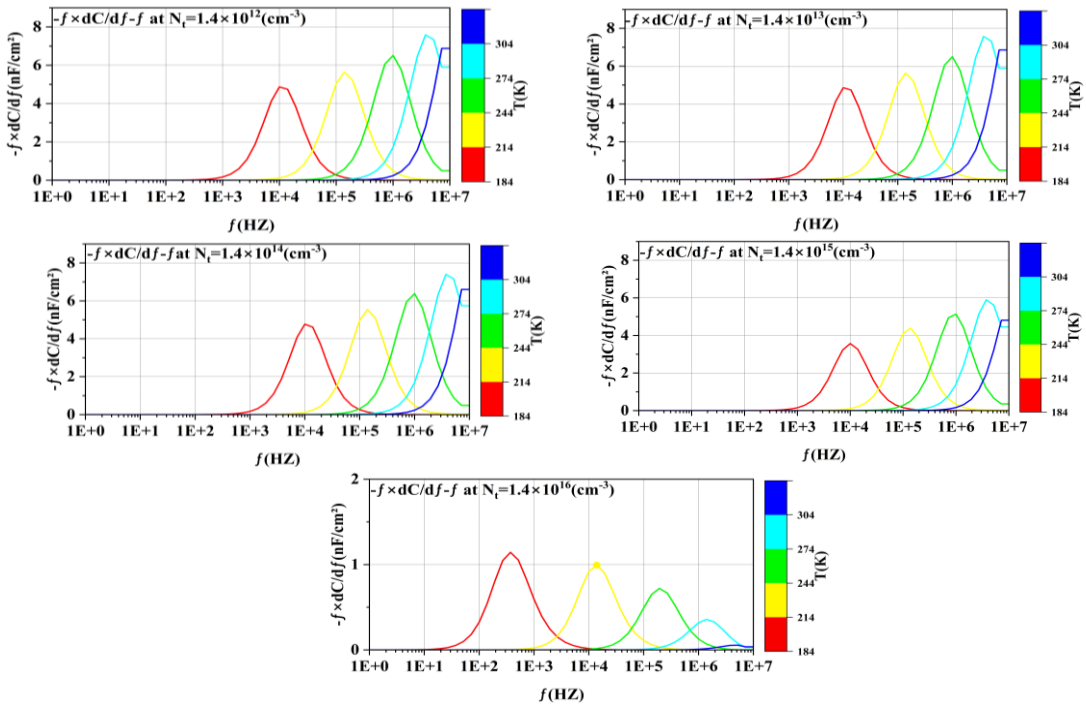

Figure 4. Temperature -dependent capacitance derivative characteristics of the CIGS solar cell under Temperatures at a different bulk defect Concentration (a)- N_t= 1.4 × 10^{12} cm^{-3}, (b)- N_t= 1.4 × 10^{13} cm^{-3} (c)- N_t= 1.4 × 10^{14} cm^{-3} (d)- N_t= 1.4 × 10^{15} cm^{-3} (e)- N_t= 1.4 × 10^{16} cm^{-3}.

Figure 5 shows the Arrhenius diagram generated from the characteristic frequencies calculated from Figure 4. A strong linear pattern is observed, indicating that the emission mechanism is thermally activated. Based on the slope of the corresponding line, the activation energy of the dominant defect level is calculated to be approximately (0.328 eV). This value is lower than the defect energy (0.88 eV) input in the simulation. This is because admittance spectroscopy considers the effective emission barrier relative to the conduction band, rather than the absolute position of the defect within the band gap. Therefore, the extracted activation energy translates to the difference in energy directed by the charge carrier emissions to the conduction band. The uniformity of activation energy across different defect Concentrations proves that the defect energy level remains constant and defect concentration only affects the strength of the amplitude response. Another good linear characteristic of the Arrhenius diagram is the presence of a single dominant defect level, which validates the physical reliability of the model and confirms that the observed amplitude transitions are due to intrinsic defects in the material [17].

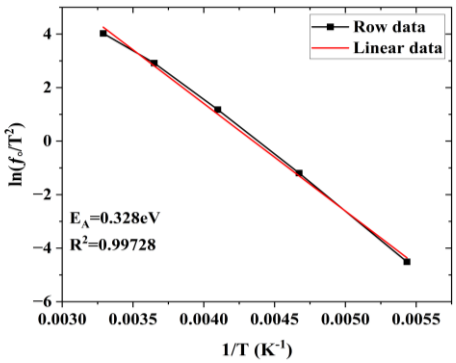

Figure 5. Arrhenius representation constructed using the data extracted from Fig. 7(c). Each data point corresponds to the characteristic defect frequency determined at a specific temperature.

4. Conclusions

In this study, the relationship between temperature (184–304 K) and defect Concentration (1.4×10^{12}–1.4×10^{16} cm^{-3}) and its effect on the capacitance behavior of a calibrated CIGS solar cell was investigated using SCAPS-1D via admittance spectroscopy. The results clearly showed that temperature is the main driver of the dynamic response of the defect states. As the temperature increases, the emission rate of the confined charge carriers increases significantly, accompanied by a uniform shift in the capacitance transition region from about (10^3 Hz) at (184 K) to about (10^6 Hz) at (304 K), and a similar shift in the characteristic frequency from about (~3.7×10^2 Hz) at (184 K) to (~5.1×10^6 Hz) at (304 K), representing an increase of approximately three orders of magnitude. At low frequencies (≤10^2 Hz), the capacitance decreases from approximately 65.7 to approximately 61.4 nF/cm² with increasing defect Concentration, indicating improved charge storage capacity with the help of traps. In the mid-frequency range (approximately 10^3 to 10^6 Hz), the response is dominated by thermal shift, attributed to thermally activated charge carrier emission. At high frequencies (≥10^6 Hz), the capacitance stabilizes at approximately (39.6 to 42 nF/cm²) and is almost unaffected by temperature or defect Concentration, indicating the dominance of depletion capacitance. Derivative analysis ($-f\mathrm{d}C/\mathrm{d}f$) allows for the precise and reproducible extraction of characteristic features and the identification of peak positions at different temperatures, where the peak positions gradually change with temperature and their intensity increases with increasing defect Concentration. The highest defect Concentration (1.4×10^{16} cm^{-3}), exhibiting distinct peaks of a single intensity, is the most reliable for determining the defect response. The activation energy derived from the Arrhenius analysis is (0.328 eV), indicating that the emission process is thermally active. This value is lower than the input defect level (0.88 eV), so the measured energy represents the effective emission barrier from the defect level to the conduction band, not the defect depth within the energy gap. The constancy of the activation energy regardless of the defect Concentration suggests that temperature influences the emission kinetics, while the defect Concentration only affects the magnitude of the electrical signal. These results also indicate that temperature controls the kinetic behavior and frequency distribution of the defect states, while the defect Concentration determines the strength and optical clarity of the response. This combined temperature and defect analysis, along with the derivation method, is an effective approach for accurately characterizing defects in CIGS solar cells.

REFERENCES

[1] P. Jackson et al., "Properties of Cu(In,Ga)Se2 solar cells with efficiencies up to 23.35%," Nature Energy, vol. 1, no. 8, pp. 1–9, 2016. https://doi.org/10.1038/nenergy.2016.57

[2] M. A. Green et al., "Solar cell efficiency tables (Version 61)," Progress in Photovoltaics, vol. 31, no. 1, pp. 3–16, 2023. https://doi.org/10.1002/pip.3646

[3] S. Siebentritt and U. Rau, Wide-Gap Chalcopyrites. Berlin, Germany: Springer, 2006. https://doi.org/10.1007/3-540-34503-4

[4] T. Walter et al., "Determination of defect distributions from admittance measurements and application to Cu(In,Ga)Se2-based heterojunctions," J. Appl. Phys., vol. 80, no. 8, pp. 4411–4420, 1996. https://doi.org/10.1063/1.363401

[5] M. Burgelman et al., "Modelling thin-film PV devices," Progress in Photovoltaics, vol. 12, no. 2–3, pp. 143–153, 2004. https://doi.org/10.1002/pip.524

[6] J. Lauwaert et al., "Impact of series resistance on capacitance spectroscopy of thin-film solar cells," Solar Energy Materials & Solar Cells, vol. 112, pp. 78–83, 2013. https://doi.org/10.1016/j.solmat.2013.01.011

[7] G. Brammertz et al., "Bias-Dependent Admittance Spectroscopy of Thin-Film Solar Cells: Experiment and Simulation," IEEE Journal of Photovoltaics, vol. 10, no. 4, pp. 1102–1111, 2020. https://doi.org/10.1109/JPHOTOV.2020.2992350

[8] S. M. Sze and K. K. Ng, Physics of Semiconductor Devices, 3rd ed. Hoboken, NJ, USA: Wiley, 2007. https://doi.org/10.1002/0470068329

[9] W. Shockley and W. T. Read, "Statistics of the recombinations of holes and electrons," Physical Review, vol. 87, no. 5, pp. 835–842, 1952. https://doi.org/10.1103/PhysRev.87.835

[10] M. J. Ahmed and A. N. Saleh, "Influence of bulk defects in SnS absorber layer on optical and electrical properties of solar cell," Journal of Physics: Conference Series, vol. 2114, no. 1, p. 012044, 2021. https://doi.org/10.1088/1742-6596/2114/1/012044

[11] H. T. Ghanem, A. N. Saleh, and M. A. Kamil, "Simulation and improvement of the efficiency of the CFTS solar cell using SCAPS-1D," Karbala International Journal of Modern Science, vol. 8, no. 1, Art. no. 7, 2022. https://doi.org/10.33640/2405-609X.3207

[12] R. L. Garris, S. Johnston, J. V. Li, H. L. Guthrey, K. Ramanathan, and L. M. Mansfield, "Electrical characterization and comparison of CIGS solar cells made with different structures and fabrication techniques," Solar Energy Materials and Solar Cells, vol. 174, pp. 77–83, 2018. https://doi.org/10.1016/j.solmat.2017.08.027

[13] S. Ouédraogo, F. Zougmoré, and J. M. B. Ndjaka, "Computational analysis of the effect of the surface defect layer (SDL) properties on Cu(In1−xGax)Se2 based solar cell performances," Journal of Physics and Chemistry of Solids, vol. 75, no. 5, pp. 688–695, 2014. https://doi.org/10.1016/j.jpcs.2014.01.010

[14] J. Pettersson, C. Platzer-Björkman, U. Zimmermann, and M. Edoff, "Baseline model of graded-absorber Cu(In,Ga)Se2 solar cells applied to cells with Zn1−xMgxO buffer layers," Thin Solid Films, vol. 519, no. 21, pp. 7476–7480, 2011. https://doi.org/10.1016/j.tsf.2010.12.141

[15] T. Eisenbarth, T. Unold, R. Caballero, C. A. Kaufmann, and H.-W. Schock, "Interpretation of admittance, capacitance-voltage, and current-voltage signatures in Cu(In,Ga)Se2 thin film solar cells," Journal of Applied Physics, vol. 107, no. 3, p. 034509, Feb. 2010. https://doi.org/10.1063/1.3277043

[16] J. Heath and P. Zabierowski, "Capacitance Spectroscopy of Thin-Film Solar Cells," in Advanced Characterization Techniques for Thin Film Solar Cells, D. Abou-Ras, T. Kirchartz, and U. Rau, Eds. Weinheim, Germany: Wiley-VCH, 2011, pp. 81–105. https://doi.org/10.1002/9783527636280.ch4

[17] J. Parion, R. Scaffidi, D. Flandre, G. Brammertz, and B. Vermang, "Low-temperature admittance spectroscopy for defect characterization in Cu(In,Ga)$(S,Se)_2$ thin-film solar cells," in Proc. 2019 IEEE 46th Photovolt. Spec. Conf. (PVSC), Chicago, IL, USA, 2019, pp. 2487-2492. https://doi.org/10.1109/PVSC40753.2019.8981249